DOI: 10.1111/nyas.15195

ORIGINAL ARTICLE

ANNALS OF THE NEW YORK ACADEMY OF SCIENCES

Capillary adhesion of stick insects

Guillermo J. Amador[1] | Brett Klaassen van Oorschot[1] | Uddalok Sen[2] | Benjamin Karman[3] | Rutger Leenders[1]

[1]Experimental Zoology Group, Wageningen University & Research, Wageningen, The Netherlands

[2]Physical Chemistry and Soft Matter, Wageningen University & Research, Wageningen, The Netherlands

[3]Biology Department, Vrije Universiteit Amsterdam, Amsterdam, The Netherlands

Correspondence
Guillermo J. Amador, Experimental Zoology Group, Wageningen University, and Research, Wageningen 6708 WD, The Netherlands.
Email: guillermo.amador@wur.nl

Funding information
Nederlandse Organisatie voor Wetenschappelijk Onderzoek, Grant/Award Number: VI.Vidi.213.122; Wageningen Institute of Animal Sciences, Wageningen University and Research, Grant/Award Number: Postdoc Talent Programme

Abstract

Scientific progress within the last few decades has revealed the functional morphology of an insect's sticky footpads—a compliant pad that secretes thin liquid films. However, the physico-chemical mechanisms underlying their adhesion remain elusive. Here, we explore these underlying mechanisms by simultaneously measuring adhesive force and contact geometry of the adhesive footpads of live, tethered Indian stick insects, *Carausius morosus*, spanning more than two orders of magnitude in body mass. We find that the adhesive force we measure is similar to the previous measurements that use a centrifuge. Our measurements afford us the opportunity to directly probe the adhesive stress in vivo and use existing theory on capillary adhesion to predict the surface tension of the secreted liquid and compare it to previous assumptions. From our predictions, we find that the surface tension required to generate the adhesive stresses we observed ranges between 0.68 and 12 mN m^{-1}. The low surface tension of the liquid would enhance the wetting of the stick insect's footpads and promote their ability to conform to various substrates. Our insights may inform the biomimetic design of capillary-based, reversible adhesives and motivate future studies on the physico-chemical properties of the secreted liquid.

KEYWORDS
adhesive pads, allometry, attachment, elastocapillary, Laplace pressure, shear force, wet adhesion

INTRODUCTION

Nature is often the source of inspiration for developing new technologies, leading to the growth of the field of biomimetics,[1] and adhesion is not an exception. Adhesion is the ability of a substance to stick (or adhere) to a dissimilar substance. Some species of insects can generate enormous adhesive forces. For example, Asian weaver ants (*Oecophylla smaragdina*) have been observed to adhere to glass substrates upside down while supporting loads more than 100 times their own body weight.[2] Over the course of their lifetime, insects adhere to a multitude of substrates of varying roughness and wettabilities.[3–5] The versatility of insect adhesion mechanisms is promising for applications involving bioinspired adhesives,[6] particularly in the design of robotic manipulators and climbers.[7]

Any adhesive should primarily satisfy two requirements: (i) establish good contact with the substrate, even in the presence of roughness, and (ii) dissipate a significant amount of energy during separation.[8] However, it is expected that modern (and future) adhesives would do more than just stick,[9] leading to a surge in recent years toward understanding and developing newer adhesion mechanisms. The advancement of microscopes along with the development of superior analytical tools has led to a renewed interest among biologists and engineers toward the development of biomimetic adhesives.[10] Nonetheless, before one delves deeper into the engineering details of biomimetic

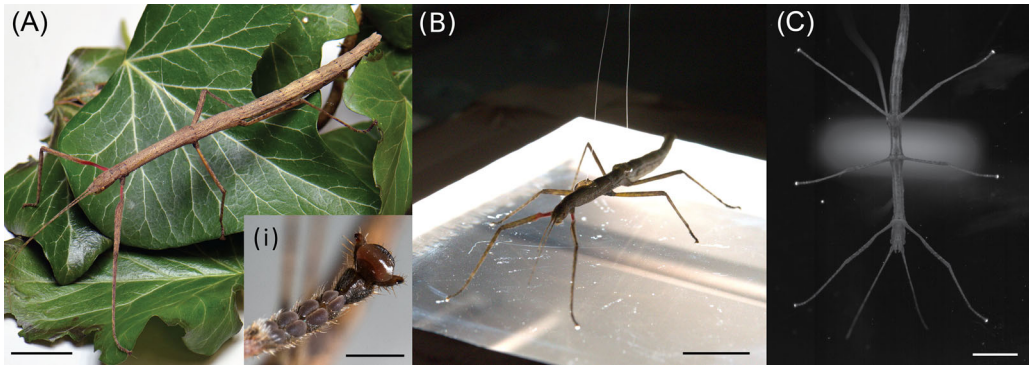

FIGURE 1 (A) An Indian stick insect (*Carausius morosus*) and (i) its distal tarsal pads, including the most distal arolium, which is used for generating adhesion. (B) A tethered insect on the frustrated total internal reflection (FTIR) experimental setup (see Figure 2 for details). (C) The view of the insect through the FTIR setup, where the arolia reflect the trapped light when in contact with the glass substrate. Scale bars represent: (A–C) 20 mm and (i) 1 mm.

adhesion, there are several fundamental questions that need answers.[2] Although high-precision characterization techniques such as atomic force microscopy and scanning electron microscopy have enabled biologists to examine the topology of the insect footpads down to the nanometer-scale, the detailed mechanisms of biological adhesion are still not fully understood,[11] particularly what the underlying physics and chemistry are and how to represent them in a mathematical model.

In order to stick to natural surfaces, certain insects, like the Indian stick insect (*Carausius morosus*), shown in Figure 1A, have developed smooth and wet adhesive pads on their feet, or arolia, which are unlike the hairy and dry adhesive pads observed on the toes of geckos.[12] To facilitate wet adhesion, smooth adhesive pads secrete an adhesive liquid into the contact zone between the pad and the substrate.[2] The contact is mediated by a nanometer-thin film of this adhesive liquid, which increases the pad's effective contact area.[2] This indicates that the smallest length scale of the adhesive pad for wet adhesion can be much higher than that for pads employing dry adhesion since the adhesive fluid in the former case helps maintain close contact with the cracks, crevices, and asperities of the rough substrate.[11] This is a clear advantage for biomimetic adhesive pads based on wet adhesion, since larger microstructures are easier to fabricate in a reproducible manner. However, the strength of capillary adhesion is greatly influenced by substrate roughness and environmental humidity.[13–17]

The typical models of wet adhesion of insects consider two undeformable flat substrates, separated by a continuous liquid layer.[18,19] A liquid bridge is formed between the two surfaces, and the total adhesive force is simply given by the sum of the surface tension, Laplace pressure, and viscous Stefan adhesion.[20] However, the major drawback of such a system lies in the low adhesive strengths (~ 1 MPa) that can be achieved as compared to dry adhesion (~ 20 MPa).[21,22] The difference can be overcome by making the adhesive pads deformable.[23]

Insects and tree frogs have been observed to have soft adhesive pads[24] with a sponge-like structure.[3] A soft adhesive pad (with a low elastic modulus) deforms more easily at a given external force, resulting in a larger contact area.[25] This higher contact area in turn increases the contact radius of the mediating liquid as the liquid is pressed toward the outside of the pad, which then increases the capillary force.[26] The Young's modulus of the soft pad also plays a role in determining the capillary tension.[27] However, this deformability invalidates existing adhesion models that rely on viscous Stefan adhesion, which only considers undeformable substrates.[3] In the past few years, there have been a few studies[28–30] on the liquid-mediated adhesion between two soft elastic substrates. However, the existing models are not based on in situ measurements of live insects, thus suggesting that there is room for improvement.

For an adhesive pad of area A that must support a mass m, the following scaling is expected: $A\sigma \sim m$,[31] where σ is the adhesive strength (or stress) of the pad. However, this follows the assumption that the nature of the adhesive force acts per unit area, akin to a Laplace pressure or constant adhesive stress. Moreover, the total available area of biological adhesive pads was found to exhibit positive allometry, with the area A scaling directly with the mass m of the organism, or $A \sim m^1$,[31] which implies that $\sigma \sim m^0$, that is, biological adhesive pads generate the same adhesive strength regardless of size and species. However, this means that the adhesive pad area A then increases disproportionately with body mass m. Indeed, as Labonte et al.[31] pointed out, if we extrapolate this to a human, nearly half of their total surface area would need to be adhesive in order to fully support their weight, which is, of course, not desirable if one wants to scale up an adhesive system.

On the other hand, in the same work,[31] it was found that this direct scaling between A and m only holds true across all animals possessing such adhesive pads, that is, insects, arachnids, reptiles, and mammals, whereas adhesive pad area was found to scale isometrically, or $A \sim m^{2/3}$, within respective phylogenetic levels. Therefore, phylogenetic inertia (or phylogenetic constraint), or the tendency for previous adaptations to influence future adaptations,[32,33] seems to limit how large adhesive pads can grow within a clade. This issue of scaling gives rise to the following questions: (i) Do adhesive pads in whole insects exhibit the same stickiness, or adhesive stress, across size (or body mass)? (ii) Are existing mathematical models of capillary-based adhesion capable of predicting the adhesive performance of stick insects? And, (iii) what are the desired physical properties of the secreted liquid in order to adhere to smooth substrates?

In this paper, we address these questions through a combination of tethering experiments to measure the adhesive force of whole insects (Figure 1B), frustrated total internal reflection (FTIR) for visualizing the contact geometry of the insects' adhesive footpads (Figure 1C), and mathematical modeling to interpret the results and predict the physical properties of the secreted liquid in order to inform the design of biomimetic adhesives. The experiments are conducted with live Indian stick insects (*C. morosus*) spanning their life cycle and more than two orders of magnitude in size (body mass m), with simultaneous and synchronized force and FTIR measurements to directly probe the relationship between adhesive force F, contact area A, adhesive stress σ, contact perimeter P, pad sliding distance δ, and body mass m.

MATERIALS AND METHODS

Study animals

Female Indian stick insects (*C. morosus*; $n = 63$ used in this study) were obtained as nymphs from Mierenboerderij (Apeldoorn, The Netherlands https://www.mierenboerderij.nl/). They were kept at 22.5°C and 50% relative humidity, and were fed European ivy (*Hedera helix*) that was picked from around Wageningen University in Wageningen, The Netherlands.

Tethering animals

In order to tether an insect for an experiment, the insect was first sedated using CO_2, unless it was a fully grown adult ($m > 500$ mg) and sedation was not necessary. For sedation, the insect was placed on a porous block and CO_2 was infused at a volumetric flow rate of approximately 1.0 m^3/h. After the stick insect was sedated, two ends of a fishing line (Nanofil size 0.04, with 0.0545-mm diameter) were fastened to both ends of the dorsal side of the thorax of the insect using UV-curable glue (Norland optical adhesive, type 60). The fishing line was glued between their hindlimbs and forelimbs, as depicted in Figure 1B, to apply a pulling force equally across the limbs and prevent pitching rotation of the body. Then, their body mass m was measured with a precision mass balance (Ohaus Corporation Adventurer Pro AV114CU, with 0.1 mg resolution).

Force measurements and FTIR

A tethered and awakened (~ 10 min after sedation) stick insect was positioned on the borosilicate glass plate in the test setup (Figure 2A). The glass plate had LED strips along each side and was mounted on a table with a rectangular hole. A high-speed camera (Mikrotron EoSens 25CXP) was mounted underneath the table to take recordings of the contact geometry of the stick insects. For the smaller stick insects ($m <$ 50 mg), a Nikon AF Micro Nikkor 105 mm f/2.8 lens was used, with a spatial resolution of 19 μm px^{-1}, while, for the larger stick insects ($m > 50$ mg), a Nikon AF Nikkor 50 mm f/1.8D lens was used, with a spatial resolution of 44 μm px^{-1}.

MATLAB (R2015b) was used to control a linear motor (Thorlabs, Z825B) that pulled the tethered insect across a distance of 25 mm vertically upward from the glass plate. A 3D-printed hook was affixed at the end of the tether to pull onto the stick insect via the tethering wire. Both the high-speed camera and the tether were synchronized by starting the filming, force recording, and pulling procedure at the same time. Each experiment lasted 25 s, with a pulling speed of 1 mm s^{-1}. The experiments were conducted at 21.0 – 25.8 °C and 26 – 61 % relative humidity.

A force transducer (Futek LSB200, 10-gram capacity) measured the force pulling on the insect at a sampling rate of 1000 Hz. Before the experiment, the force transducer was calibrated with four different weights. The slope of the linear regression line through the four data points was used to calculate force (in mN) from the measured change in the electrical voltage (in mV V^{-1}) by the transducer. Figure S1 shows the calibration data and the linear regression. The measured pulling force for each insect was filtered using a moving average filter with a window size of 25, and the peak (or maximum) force was extracted. Following a free-body diagram, the insect's weight mg was subtracted from the peak force to obtain the adhesive force F. The temporal variation of the pulling force from a typical experiment is shown in Figure 2B. Figure S2 shows two other examples from the smallest ($m = 4.9$ mg) and largest ($m = 1200$ mg) insects used in the study.

The contact area was captured by the high-speed camera at 124 Hz with 5-MP resolution using FTIR. A light beam will mostly reflect internally when it is shone into a medium that has a higher index of reflection compared to the air surrounding it. However, when another object with a similar index of refraction comes into contact with the medium, then some of the total internal reflection will be frustrated and scatter out of the medium. FTIR was used to visualize the contact geometry of the adhesive pads on the glass plate, so that the contact area A and contact perimeter P could be quantified.

Using the filtered force measurement, the time of peak force was obtained and the associated image was analyzed in MATLAB (R2018b) to obtain A and P at the point of peak force generation. In order to quantify these parameters, the image was binarized using a threshold of 0.5. Then, the center of each pad was identified by manual clicking, and a square region of 30 by 30 pixels (enough to encompass each entire pad) was drawn around each pad. Typical images obtained using the FTIR method are shown in Figure 2C–E, with the raw images on the left (i) and binarized images on the right (ii).

To obtain the contact area A, the total number of pixels within each square was summed and combined with a calibration value to obtain the contact area of each pad. The area of the pads from all the limbs of the insect was summed to determine the total contact area A. Finally, to obtain the contact perimeter P, the *bwperim* function in MATLAB (R2018b) was used to calculate the perimeter of each pad and then summed.

Using both force and contact geometry measurements, the adhesive stress σ was determined using the following expression:

$$\sigma = \frac{F}{A}. \quad (1)$$

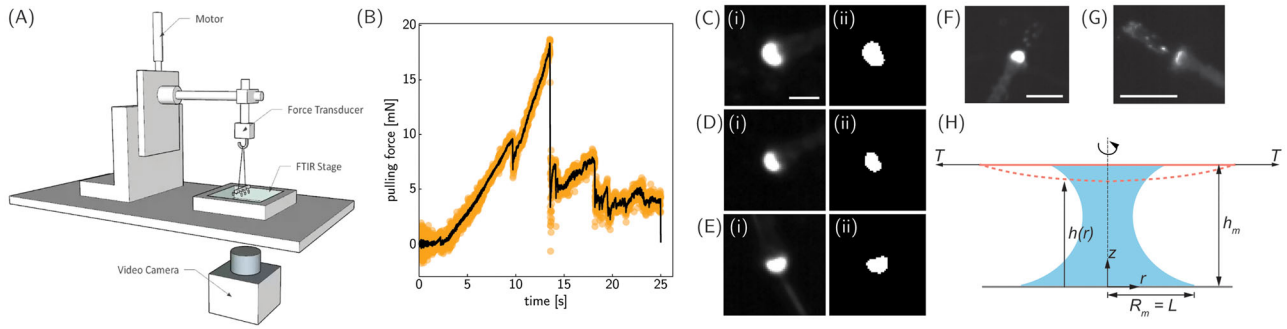

FIGURE 2 (A) Schematic of the experimental setup combining tethered pulling measurements with frustrated total internal reflection (FTIR) imaging. (B) Pulling force measurement for a typical experiment with an insect of mass $m = 390$ mg. The discrete data points in yellow represent the experimental measurements, while the solid black line denotes the filtered data. The adhesive force F is taken as the peak force minus the insect's weight. (C–E) Images of three adhesive pads, from the same insect as in panel B, using FTIR with (i) raw and (ii) binarized images. The binarized images are used for quantifying the contact area A and the contact perimeter P. The scale bar represents 1 mm. (F) Image of a footpad after sliding, from the same insect as in panels B–E. The scale bar represents 2 mm. (G) Image of a footpad after sliding, from an insect with $m = 21$ mg. The scale bar represents 1 mm. (H) Schematic for mathematical modeling, inspired by Butler et al.[30] Here, the solid pink line denotes the undeformed footpad, while the dashed pink line represents the deformed footpad. The liquid bridge is represented in blue, while the gray line denotes the substrate to which the insect is adhering. Variables are defined in the text.

TABLE 1 Summary of the power-law fits for measurements shown in Figure 3A–D.

Parameter	Unit	Power-law exponent	95% CI	R^2
Contact area A	mm^2	0.77	(0.69, 0.85)	0.86
Adhesive force F	mN	0.55	(0.49, 0.60)	0.87
Adhesive stress σ	kPa	−0.22	(−0.31, −0.13)	0.27
Contact perimeter P	mm	0.41	(0.35, 0.46)	0.79

Abbreviations: CI, confidence interval; R^2, coefficient of determination.

Power law fitting

After the adhesive force F, contact area A, contact perimeter P, and adhesive stress σ were determined for each insect of mass m, the data were log-transformed in order to determine the best-fitting power law. The log-transformed data were fitted using a linear regression, with the slope of the regression representing the exponent of the best fitting power law. The data were plotted in log-log axes along with the best power-law fits in Figure 3A–D, and the power-law exponents with 95% confidence interval (CI) and coefficient of determination R^2 are shown in Table 1.

Measurements of footpad sliding

Using the synchronized high-speed videos from the FTIR setup, we quantified the sliding distance δ of the footpads of the stick insects. After finding the video frame associated with the point of maximum adhesive force F, the frame when the footpads started to slide was found for each trial. Then, using the *imshowpair* function in MATLAB (R2018b), the two images (at the onset of sliding and when maximum force occurred) were overlaid and the sliding distance of each footpad was measured by clicking the center of each footpad before and after sliding. Finally, the sliding distances of the six footpads were averaged for an individual and reported as the sliding distance δ (Figure 3F). Figure 2F,G shows images of footpads after sliding.

Mathematical model

The stick insects studied in the current work have smooth, deformable footpads that secrete a liquid. Thus, they create a liquid bridge between the pad and the substrate, and make use of the elastocapillarity-induced adhesion arising from both the elasticity of the deformable footpad and the capillarity of the liquid bridge. The fluid dynamics of this particular scenario has been recently studied by Butler et al.[30] In what follows, we briefly describe the model used in our study, which is largely based on the model proposed by Butler et al.[30], and the assumptions and modifications we made.

The schematic of the model geometry is shown in Figure 2H. We consider the insect footpad to be a circular, deformable membrane of constant thickness and having Young's modulus E. We restrict ourselves to small axisymmetric deformations of the membrane about the coordinate system shown in Figure 2H. We assume that the imposed tension T on the footpad by the insect is uniform, and that the ends of the membrane (footpad) are fixed at the radial position $r = L$. Hence, by modulating the tension T, the insect can only change the curvature of the membrane. Note that, in reality, T can change due to the vertical deformation of the membrane, but we neglect that here for simplicity (also following Butler et al.[30]). The insect adheres to a flat, smooth, and rigid substrate at a vertical distance h_M from the membrane by secreting a liquid of volume V and surface tension γ between the membrane and the substrate. From previous experiments,[19] we know that the distance between the membrane and the substrate is small, which means that the aspect ratio $h_M/L \ll 1$. Note that we exaggerate this

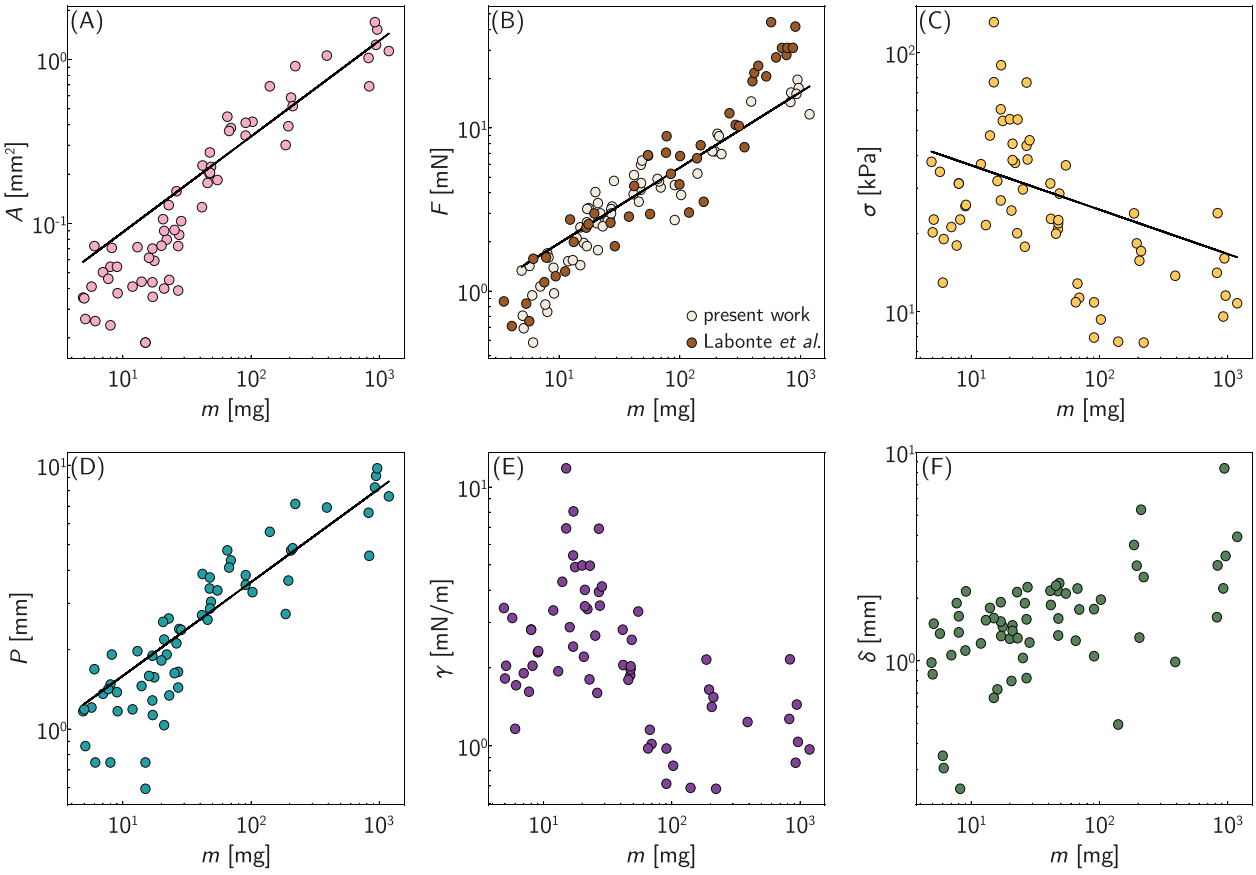

FIGURE 3 Measurements of: (A) contact area A, (B) adhesive force F, (C) adhesive stress σ, (D) contact perimeter P, (E) liquid tension γ, and (F) sliding distance δ across body mass m. The solid lines denote power-law fits, provided in Table 1. Panel B also shows the whole-insect centrifuge measurements from Labonte et al.[40] The data for this figure is provided in Table S1.

gap in Figure 2H for clarity. Previous studies[34] suggested that the secreted liquid volume V is small; hence, gravity can be neglected in the mathematical formulation.

The interfacial tension γ of the liquid bridge formed between the membrane and the substrate results in a capillary force due to the pressure difference between the inside and the outside of the liquid volume. This pressure difference is proportional to the curvature of the liquid bridge. We further assume that the liquid secretion perfectly wets the footpad, as supported by previous studies that found the liquid secreted by the pads is also secreted throughout the rest of the body.[35] Hence, the liquid covers the entire surface area of the membrane (note that Figure 2H shows the more generalized case where the liquid only partially wets the membrane). The interfacial tension is expected to contribute to a discontinuity of the membrane tension at the membrane-liquid contact line,[30] but this is neglected here as $T \gg \gamma$. While smooth adhesive pads of insects are soft in compression, in order to conform to rough substrates, their internal fibrillar structure provides high resistance to tension.[36]

For the squeezed thin liquid bridge ($h_M/L \ll 1$) in the present scenario, we can assume that the axial curvature dominates over the azimuthal curvature in determining the capillary force.[37] We further approximate the meniscus cross-section to be a circular arc of radius $h_M/2$ (since the liquid is perfectly wetting the membrane and the substrate with very low contact angles[19]).[30] The capillary pressure at the meniscus (relative to the atmospheric pressure) can then be written as:

$$p_M = -\frac{2\gamma}{h_M}. \tag{2}$$

Before we discuss adhesion with a deformable membrane, it is worth visiting the classical limit of adhesion with a rigid membrane, that is, when $T \to \infty$. The adhesive force results from the capillary pressure p_M acting over an area $A = V/h_M$, and is given by

$$F_{\text{rigid}} = 2\gamma\frac{V}{h_M^2}. \tag{3}$$

Thus, the adhesive force in this case is purely governed by the separation gap h_M.

Let us now consider the deformable membrane, which is the relevant scenario in the present case. For the axisymmetric coordinate system shown in Figure 2H, the membrane position is described by $z = h(r, t)$ with the substrate at $z = 0$, where r is the radial coordinate, z is the axial coordinate, and t is the time. We consider the static scenario (i.e., no flow within the liquid volume) where the pressure field $p(r, t)$ within the liquid is uniform, and the membrane shape $h(r, t)$, determined

by a local force balance, is a solution of the Young–Laplace equation:

$$\frac{T}{r}\frac{\partial}{\partial r}\left(r\frac{\partial h}{\partial r}\right) = -p, \tag{4}$$

where we have assumed a small membrane slope because of the small aspect ratio ($h_M/L \ll 1$) and neglected the inertia of the membrane.

The secreted liquid volume is also constant, which results in the following conservation equation:

$$V = 2\pi \int_0^L rh\,\mathrm{d}r, \tag{5}$$

where we have assumed that the meniscus shape has a negligible effect on the volume due to the small aspect ratio ($h_M \ll L$).

Since we consider here the equilibrium scenario where there is no flow within the liquid volume, the pressure within the liquid p must be uniform and equal to the pressure at the meniscus, p_M (given by Equation (2)). Hence, Equation (4) can be rewritten as:

$$\frac{1}{r}\frac{\partial}{\partial r}\left(r\frac{\partial h}{\partial r}\right) = \frac{2\gamma}{Th_M}, \tag{6}$$

subject to the boundary conditions arising from the imposed symmetry at $r = 0$ and the meniscus position at $r = r_M$ (note that here $r_M = L$ since we have assumed that the liquid perfectly wets the membrane):

$$\frac{dh}{dr} = 0 \quad \text{at} \quad r = 0 \quad \text{and} \tag{7}$$

$$h = h_M \quad \text{at} \quad r = r_M. \tag{8}$$

The governing equation (6), along with the boundary conditions (7) and (8), leads to the radial height profile given by

$$h = \frac{\gamma}{Th_M}\left(\frac{r^2 - r_M^2}{2} + h_M^2\right). \tag{9}$$

While all of these are interesting for understanding the contact mechanics, perhaps the quantity most relevant to the present research is the adhesive force F. We restrict ourselves to the "non-contacting" scenario,[30] where the membrane does not touch the substrate, that is, there is always a thin liquid layer between the membrane and the substrate. In such a case, following from Equation (3), the adhesive force can be expressed as:

$$F = 2\pi\gamma\frac{r_M^2}{h_M}, \tag{10}$$

which indicates that the adhesive force scales with the square of the contact radius but inversely with the liquid film thickness. In what follows, we use this result to rationalize our experimental findings and discuss their implications.

RESULTS

By combining the tethered force measurements with the FTIR images, the adhesive force and pad contact geometry were measured simultaneously for $n = 63$ Indian stick insects varying in body mass m from 4.9 to 1200 mg. The results are shown in Figure 3, with the power-law fittings provided in Table 1.

For contact area A (Figure 3A), it was found to scale as $m^{0.77}$ (95% CI: [0.69, 0.85] and $R^2 = 0.86$), while adhesive force F (Figure 3B) was found to scale as $m^{0.55}$ (95% CI: [0.49, 0.60] and $R^2 = 0.87$). The combination of these two scalings, via Equation (1), reflects what was found for adhesive stress σ (Figure 3C), which scaled as $m^{-0.22}$ (95% CI: [−0.31, −0.13] and $R^2 = 0.27$). Therefore, the adhesive strength of the pads decreased as the insects grew in size. Spearman's rank correlation indicated that stress σ and mass m were correlated with a decreasing trend ($\rho = -0.52$ and $p < 0.001$). The contact perimeter P (Figure 3D) was found to scale as $m^{0.41}$ (95% CI: [0.35, 0.46] and $R^2 = 0.79$).

Using the mathematical model (Equation (10)), the surface tension γ of the adhesive liquid secretion was predicted (Figure 3E). The height h_M of the liquid layer was assumed to be 90 nm, as previously measured using interferometry.[19] The predicted surface tension γ ranged between 0.68 and 12 mN m^{-1}. This is lower than the surface tension for oil-based liquids of approximately 20 mN m^{-1}, which is the value typically assumed for the secreted liquid.[38,39] If we instead assume surface tension $\gamma = 20$ mN m^{-1}, then the predictions of liquid height h_M range from 150 to 2600 nm, which are greater than those measured using interferometry (90– 160 nm).[19]

Figure 3F shows how sliding distance δ, which is associated with the shearing of the footpads, varies with body mass m. In the live insects, we observed a similar relationship as was reported for the controlled, single-pad measurements from Labonte et al.[40] The sliding distance δ was relatively constant for small insects and then increased for larger insects. Using Spearman's rank correlation, we found that sliding distance δ and mass m were correlated with an increasing trend ($\rho = 0.52$ and $p < 0.001$).

DISCUSSION

The adhesive pad area was previously measured for various animals using microscopic images.[31] For Indian stick insects, the area was found to scale as $m^{0.70}$, following what is expected from isometry, with area scaling as $m^{2/3}$. The measurements reported here show a scaling relationship slightly higher than isometry, but with the lower bound of the 95% confidence interval overlapping with the previous pad area measurements of Indian stick insects from Labonte et al.[31] In addition to quantifying contact area A, we measured the contact perimeter P of the pads and found that the perimeter $P \sim A^{1/2}$, as expected from isometry.

Previous research investigated the scaling of Indian stick insect adhesion by combining whole-insect experiments with a centrifuge and single-pad measurements with a motorized stage and feedback loop.[40] In this previous work, it was found that the adhesive force $F \sim m^{0.69}$ (95% CI: [0.59, 0.79]) in whole insects. For single pads, $F \sim m^{0.34}$

(95% CI: [0.27, 0.40]) without shearing, $F \sim m^{0.71}$ (95% CI: [0.61, 0.82]) with a shear force proportional to $m^{2/3}$, and $F \sim m^{0.87}$ (95% CI: [0.70, 1.03]) with a shear force proportional to m^1. While the forces measured here are similar to those reported for the centrifuge measurements (see Figure 3B), the scaling with mass differs slightly, with a small overlap of the 95% confidence intervals.

In our direct measurements, we observed that the adhesive stress σ decreased with body mass m, albeit with a poor goodness of fit ($R^2 = 0.27$). Therefore, it is possible that σ is instead independent of body mass m. According to Labonte et al.[40], if the stress σ decreases with mass m, or $\sigma \sim m^{-1/3}$, it would indicate that the insects are not shearing their adhesive pads. However, as shown in Figures 2F,G and 3F, the insect pads were observed to shear, with the sliding distance δ varying between 0.24 and 8.4 mm, which is significantly higher than the range of sliding distances reported for the single-pad measurements in Ref. 40 (0–2 mm). Similarly, a previous study on beetles[41] observed greater sliding distances in live, freely climbing beetles when compared to controlled single-pad experiments with simulated steps.[42]

Previous mathematical models were proposed for capillary-based adhesion. However, many of them do not account for the height h_M of the liquid film. For instance, the capillary adhesion model used to predict the attachment performance of an array of small liquid bridges inspired by a leaf beetle states that $\sigma \sim P^{-1}$,[43] neglecting height altogether. While we also found a decreasing trend in the adhesive stress σ versus the size, we do not find the same inverse scaling relation between σ and the contact perimeter P. Another capillary adhesion model, based on Hertz contact theory of elastic solids with attraction effects via the extension by Johnson, Kendall, and Roberts (JKR theory), predicts that $F \sim R_c$, where R_c is the radius of curvature of the adhesive pad.[19,44] For our measurements, we find that adhesive force F does not seem to scale with pad radius (or $A^{1/2}$). However, it remains unknown whether the radius of curvature R_c scales isometrically with the body mass m.

For hairy adhesive pads with secreted liquid, like in the green dock beetle (*Gastrophysa viridula*), the elastocapillary adhesion of individual fibers was modeled using a similar capillary model as in Equation (10), based on the capillary Laplace pressure.[38] Using this model, the adhesive force that each fiber generated was predicted and found to agree with previous experiments on single fibers of the same species.[38,45]

From our predictions, based on Equation (10), we find that if the liquid height h_M is constant, then the secreted adhesive liquid does not require high surface tension in order to generate the observed adhesive stress σ. An average surface tension of $\gamma = 2.7$ mN m^{-1} was found to be sufficient, given a liquid film height $h_M = 90$ nm. Therefore, it is possible that stick insects prioritize the wettability of their secreted adhesive liquid. Insect adhesive secretions exhibit low contact angles on substrates, 17° on glass and 1.3° on hydrophobic polyimide.[19,46] Secreting a liquid with such a low surface tension may explain how versatile insect adhesion is with respect to substrate properties. A previous study with three stick insect species found that adhesive force was not significantly affected by the surface free energy of the substrate.[5] With low surface tension, the secreted liquid can easily flow into the asperities on rough substrates in order to maximize contact area. By using the capillary model proposed by Butler et al.[30] (Equation (10)), engineers can make informed decisions on the development of capillary-based adhesives, especially regarding the working liquid.

The elastocapillary adhesion model we used from Butler et al.[30] assumes a static situation, where the pad is not sliding and the secreted liquid is not flowing. We did observe significant sliding in our experiments (see Figure 3F), so future work should be dedicated to developing a dynamic model that includes the effects of shearing. Previous work has shown that the adhesive force F is linearly proportional to the shear force[40,47]; however, the mechanisms underlying this linear relationship are still unknown. Therefore, shearing should be accounted for in a more sophisticated model in order to determine if the liquid height h_M is affected by the amount of shearing and how this could relate to the size of the insect, especially since the sliding distance δ was observed to increase with mass m (Figure 3F) and the secreted liquid is deposited onto the substrate during shearing (see Figure 2F,G and Labonte et al.[40]). Moreover, the inverse relationship between the adhesive force F and the liquid height h_M has been found to not hold true when attaching to rough substrates.[23,48,49] Therefore, further developments in mathematical modeling should also aim to include the effects of substrate roughness on adhesion force.

Given the adhesive stresses observed here, we can estimate the amount of adhesive surface area that would be required for biomimetic adhesives. If a biomimetic, elastocapillary adhesive achieves the maximum stresses observed for the stick insects, $\sigma \approx 100$ kPa, it can support a kilogram of mass per cm^2 of adhesive area. This adhesive stress is comparable to adhesive stresses observed for the capillary-based gripper of Vogel and Steen[43] with pore sizes between 1 and 10 μm, as well as those measured for various gecko-inspired adhesives (i.e., mushroom-capped and microindented) that do not use liquids or glues.[50] Therefore, given the ability of capillary adhesives to conform to rough substrates without the need for micro- and nano-scopic fibers and their competitive adhesive stresses, they present a promising option for future biomimetic adhesives. However, the material properties and microstructures, as well as the working liquid, are critical for their performance, especially across a multitude of substrates. Additionally, environmental conditions, such as temperature and humidity, need to be considered.

AUTHOR CONTRIBUTIONS

G.J.A. conceived the study. G.J.A. and B.K.v.O. designed the experimental setup. G.J.A. and U.S. designed and conducted the mathematical modeling. G.J.A., B.K., and R.L. conducted the experiments. G.J.A., B.K.v.O., and U.S. wrote the manuscript. All authors reviewed and provided critical revisions to the manuscript.

ACKNOWLEDGMENTS

We thank Remco Pieters and Anne de Waal for assistance with the experimental setup, Jelle Steens and Susan van den Bos for their early contributions in designing the experiments, and David Labonte for the fruitful discussions and review of the manuscript.

COMPETING INTERESTS

The authors declare no competing interests.

ORCID

Guillermo J. Amador https://orcid.org/0000-0003-3594-125X
Brett Klaassen van Oorschot https://orcid.org/0000-0003-4347-5391

PEER REVIEW

The peer review history for this article is available at: https://publons.com/publon/10.1111/nyas.15195

REFERENCES

1. Bhushan, B. (2009). Biomimetics: Lessons from nature – An overview. *Philosophical Transactions of the Royal Society A: Mathematical, Physical and Engineering Sciences*, *367*, 1445–1486.
2. Dirks, J.-H., & Federle, W. (2011). Fluid-based adhesion in insects - Principles and challenges. *Soft Matter*, *7*, 11047–11053.
3. Gorb, S. N. (2001). *Attachment devices of insect cuticle*. Dordrecht, Boston: Kluwer Academic Publishers.
4. Stark, A. Y., & Yanoviak, S. P. (2018). Adhesion and running speed of a tropical arboreal ant (*Cephalotes atratus*) on wet substrates. *Royal Society Open Science*, *5*(11), 181540.
5. Thomas, J., Gorb, S. N., & Büscher, T. H. (2023). Influence of surface free energy of the substrate and flooded water on the attachment performance of stick insects (Phasmatodea) with different adhesive surface microstructures. *Journal of Experimental Biology*, *226*(3), jeb244295.
6. Feldmann, D., Das, R., & Pinchasik, B.-E. (2021). How can interfacial phenomena in nature inspire smaller robots. *Advanced Materials Interfaces*, *8*, 2001300.
7. Drotlef, D.-M., Dayan, C. B., & Sitti, M. (2019). Bio-inspired composite microfibers for strong and reversible adhesion on smooth surfaces. *Integrative and Comparative Biology*, *59*, 227–235.
8. Gay, C., & Leibler, L. (1999). On stickiness. *Physics Today*, *52*, 48–52.
9. Fakley, M. (2001). Smart adhesives. *Chemistry and Industry*, *5*, 691–695.
10. Smith, A. M. (2016). *Biological adhesives*. Switzerland: Springer International Publishing.
11. Federle, W. (2006). Why are so many adhesive pads hairy? *Journal of Experimental Biology*, *209*, 2611–2621.
12. Autumn, K., & Gravish, N. (2008). Gecko adhesion: Evolutionary nanotechnology. *Philosophical Transactions of the Royal Society A: Mathematical, Physical and Engineering Sciences*, *366*, 1575–1590.
13. Xiao, X., & Qian, L. (2000). Investigation of humidity-dependent capillary force. *Langmuir*, *16*(21), 8153–8158.
14. Ata, A., Rabinovich, Y. I., & Singh, R. K. (2002). Role of surface roughness in capillary adhesion. *Journal of Adhesion Science and Sechnology*, *16*(4), 337–346.
15. Köber, M., Sahagún, E., García-Mochales, P., Briones, F., Luna, M., & Sáenz, J. J. (2010). Nanogeometry matters: Unexpected decrease of capillary adhesion forces with increasing relative humidity. *Small*, *6*(23), 2725–2730.
16. Voigt, D., Schuppert, J., Dattinger, S., & Gorb, S. (2010). Temporary stay at various environmental humidities affects attachment ability of Colorado potato beetles *Leptinotarsa decemlineata* (Coleoptera, Chrysomelidae). *Journal of Zoology*, *281*(4), 227–231.
17. Heepe, L., Wolff, J. O., & Gorb, S. N. (2016). Influence of ambient humidity on the attachment ability of ladybird beetles (*Coccinella septempunctata*). *Beilstein Journal of Nanotechnology*, *7*(1), 1322–1329.
18. Walker, G. (1993). Adhesion to smooth surfaces by insects – A review. *International Journal of Adhesion and Adhesives*, *13*, 3–7.
19. Federle, W., Riehle, M., Curtis, A. S. G., & Full, R. J. (2002). An integrative study of insect adhesion: Mechanics and wet adhesion of pretarsal pads in ants. *Integrative and Comparative Biology*, *41*, 1100–1106.
20. Hanna, G., & Barnes, W. J. P. (1991). Adhesion and detachment of the toe pads of tree frogs. *Journal of Experimental Biology*, *155*, 103–125.
21. Federle, W. (2006). Why are so many adhesive pads hairy? *Journal of Experimental Biology*, *209*, 2611–2621.
22. Smith, A. M. (1991). Negative pressure generated by octopus suckers: A study of the tensile strength of water in nature. *Journal of Experimental Biology*, *157*, 257–271.
23. Dirks, J.-H. (2014). Physical principles of fluid-mediated insect attachment - Shouldn't insects slip? *Beilstein Journal of Nanotechnology*, *5*, 1160–1166.
24. Federle, W., Barnes, W. J. P., Baumgartner, W., Drechsler, P., & Smith, J. M. (2006). Wet but not slippery: Boundary friction in tree frog adhesive toe pads. *Journal of the Royal Society Interface*, *3*, 689–697.
25. Büscher, T. H., & Gorb, S. N. (2021). Physical constraints lead to parallel evolution of micro- and nanostructures of animal adhesive pads: A review. *Beilstein Journal of Nanotechnology*, *12*(1), 725–743.
26. Butt, H.-J., Barnes, W. J. P., del Campo, A., Kappl, M., & Schönfeld, F. (2010). Capillary forces between soft, elastic spheres. *Soft Matter*, *6*, 5930–5936.
27. Wexler, J. S., Heard, T. M., & Stone, H. A. (2014). Capillary bridges between soft substrates. *Physical Review Letters*, *112*, 066102.
28. Duprat, C., Protière, S., Beebe, A. Y., & Stone, H. A. (2012). Wetting of flexible fibre arrays. *Nature*, *482*, 510–513.
29. Duprat, C., Noûs, C., & Protière, S. (2020). Controlling wet adhesion with elasticity. *Soft Matter*, *16*, 6463–6467.
30. Butler, M., Box, F., Robert, T., & Vella, D. (2019). Elasto-capillary adhesion: Effect of deformability on adhesion strength and detachment. *Physical Review Fluids*, *4*, 033601.
31. Labonte, D., Clemente, C. J., D., A., Kuo, C.-Y., Crosby, A. J., Irschick, D. J., & Federle, W. (2016). Extreme positive allometry of animal adhesive pads and the size limits of adhesion-based climbing. *Proceedings of the National Academy of Sciences of the United States of America*, *113*, 1297–1302.
32. McKitrick, M. C. (1993). Phylogenetic constraint in evolutionary theory: Has it any explanatory power? *Annual Review of Ecology, Evolution, and Systematics*, *24*, 307–330.
33. Darwin, C. (1859). *The origin of species*. New York: Penguin.
34. Dirks, J.-H., Clemente, C. J., & Federle, W. (2010). Insect tricks: Two-phasic foot pad secretion prevents slipping. *Journal of the Royal Society Interface*, *7*, 587–593.
35. Geiselhardt, S. F., Geiselhardt, S., & Peschke, K. (2009). Comparison of tarsal and cuticular chemistry in the leaf beetle *Gastrophysa viridula* (Coleoptera: Chrysomelidae) and an evaluation of solid-phase microextraction and solvent extraction techniques. *Chemoecology*, *19*, 185–193.
36. Gorb, S. N. (2007). Smooth attachment devices in insects: Functional morphology and biomechanics. *Advances in Insect Physiology*, *34*, 81–115.
37. Reyssat, E. (2015). Capillary bridges between a plane and a cylindrical wall. *Journal of Fluid Mechanics*, *73*, R1.
38. Gernay, S., Federle, W., Lambert, P., & Gilet, T. (2016). Elasto-capillarity in insect fibrillar adhesion. *Journal of the Royal Society Interface*, *13*(121), 20160371.
39. Gennes, P.-G., Brochard-Wyart, F., & Quéré, D. (2004). *Capillarity and wetting phenomena: Drops, bubbles, pearls, waves*. New York: Springer.
40. Labonte, D., Struecker, M.-Y., Birn-Jeffery, A. V., & Federle, W. (2019). Shear-sensitive adhesion enables size-independent adhesive performance in stick insects. *Proceedings B of the Royal Society*, *286*, 20191327.
41. Amador, G. J., Endlein, T., & Sitti, M. (2017). Soiled adhesive pads shear clean by slipping: A robust self-cleaning mechanism in climbing beetles. *Journal of the Royal Society Interface*, *14*, 20170134.

42. Clemente, C. J., Bullock, J. M. R., Beale, A., & Federle, W. (2010). Evidence for self-cleaning in fluid-based smooth and hairy adhesive systems of insects. *Journal of Experimental Biology*, *213*, 635–642.
43. Vogel, M. J., & Steen, P. H. (2010). Capillarity-based switchable adhesion. *Proceedings of the National Academy of Sciences of the United States of America*, *107*, 3377–3381.
44. Fogden, A., & White, L. R. (1990). Contact elasticity in the presence of capillary condensation: I. The nonadhesive Hertz problem. *Journal of Colloid and Interface Science*, *138*(2), 414–430.
45. Bullock, J. M., & Federle, W. (2011). Beetle adhesive hairs differ in stiffness and stickiness: In vivo adhesion measurements on individual setae. *Naturwissenschaften*, *98*, 381–387.
46. Kaimaki, D.-M., Andrew, C. N., Attipoe, A. E., & Labonte, D. (2022). The physical properties of the stick insect pad secretion are independent of body size. *Journal of the Royal Society Interface*, *19*(191), 20220212.
47. Federle, W., & Labonte, D. (2019). Dynamic biological adhesion: Mechanisms for controlling attachment during locomotion. *Philosophical Transactions of the Royal Society B: Biological Sciences*, *374*, 20190199.
48. Baier, R. E., Shafrin, E. G., & Zisman, W. A. (1968). Adhesion: Mechanisms that assist or impede it. *Science*, *162*, 1360–1368.
49. Drechsler, P., & Federle, W. (2006). Biomechanics of smooth adhesive pads in insects: Influence of tarsal secretion on attachment performance. *Journal of Comparative Physiology A*, *192*, 1213–1222.
50. Suresh, S. A., Hajj-Ahmad, A., Hawkes, E. W., & Cutkosky, M. R. (2021). Forcing the issue: Testing gecko-inspired adhesives. *Journal of the Royal Society Interface*, *18*(174), 20200730.

SUPPORTING INFORMATION

Additional supporting information can be found online in the Supporting Information section at the end of this article.

How to cite this article: Amador, G. J., Klaassen van Oorschot, B., Sen, U., Karman, B., & Leenders, R. (2024). Capillary adhesion of stick insects. *Ann NY Acad Sci.*, *1538*, 98–106. https://doi.org/10.1111/nyas.15195